Journal of Alloys and Compounds 517 (2012) 198–203

Contents lists available at SciVerse ScienceDirect

Journal of Alloys and Compounds

journal homepage: www.elsevier.com/locate/jallcom

Fabrication and reliability evaluation of $CoSb_3$/W–Cu thermoelectric element

Degang Zhao*, Haoran Geng, Xinying Teng

School of Materials Science and Engineering, University of Jinan, Jinan 250022, China

ARTICLE INFO

Article history:
Received 25 October 2011
Received in revised form
23 December 2011
Accepted 23 December 2011
Available online 31 December 2011

Keywords:
Thermoelectric
$CoSb_3$
Spark plasma sintering
W–Cu alloy

ABSTRACT

Joining of thermoelectric material with electrode is the key technique in the construction of thermoelectric device for the practical application. In this study, a suitable W–Cu alloy electrode was introduced into $CoSb_3$-based element with insertion of Ti layer by means of spark plasma sintering. Finite element analysis showed that the maximum thermal residual stress appeared at the cylindrical surface zone close to the $CoSb_3$/electrode interface. SEM results showed that an intermetallic compound (IMC) layer formed at the $CoSb_3$/Ti interface. After accelerated thermal aging, a three-layer IMC structure was observed at the $CoSb_3$/Ti interface and EDS analysis confirmed that the IMC layers were composed of TiCoSb, $TiSb_2$ and TiSb. The $CoSb_3/Ti/W_{80}Cu_{20}$ elements had sufficient shear strength for the reliability of thermoelectric device. The contact resistance of $CoSb_3$/Ti/W–Cu was minimal and below the 50 $\mu\Omega\,cm^2$, indicating the element exhibited a good electrical contact. The reliability evaluation showed that the element had high thermal duration stability.

© 2011 Elsevier B.V. All rights reserved.

1. Introduction

Thermoelectric (TE) conversion has attracted worldwide interest for the application in electronic cooling, waste heat recovery and special power source, because it is silent in operation and highly reliable with no moving parts [1,2]. To achieve high efficiency, besides high figure-of-merit TE material and large temperature difference, the good contact property of TE material and electrode must be desired. Therefore a good TE joint should have not only good reliability but also low thermal and electrical resistivity. In the past decade, several works have been done on joining TE materials with their electrodes. Copper was soldered with TE material through brazing in Bi_2Te_3 device. For PbTe TE device, Fe and Ni were commonly used as the electrodes and joining was made by plasma activated sintering [3]. Carbon or tungsten electrode was applicable for fabricating SiGe device [4].

Recently, doped or filled $CoSb_3$-based skutterudites have been reported to have high ZT value and regarded as one of the most promising materials working at intermediate temperature region [5–8]. However, as the key technology for fabricating TE device, the joining of $CoSb_3$ TE materials with metal electrode is still an obstacle. Unlike bismuth telluride based TE device, tin soldering is not favorable for joining $CoSb_3$-based materials with electrode because of the low melting point of tin soldering. At present, Jet Propulsion Laboratory adopted solid–solid contact between copper electrode and $CoSb_3$-based TE materials and the contact was maintained by compression springs [9]. However, this method will result in high interfacial electrical resistance and thermal resistance, which could significantly decrease the output power and efficiency of device [10]. In our previous work, $CoSb_3$ material was successfully joined with Mo–Cu electrode by spark plasma sintering (SPS) and high temperature reliability evaluation was carried out through thermal duration test [11]. Recently we minimized the CTE mismatch between electrode and $CoSb_3$ material using W–Cu alloy electrodes and fabricated the $CoSb_3$/W–Cu elements. In addition, the electrical and thermal conductivity of W–Cu alloy are higher than those of Mo–Cu, indicating the $CoSb_3$/W–Cu element has low contact resistivity and thermal residual stress at the $CoSb_3$/electrode interface so that a high efficiency of energy conversion can be attained.

In this study, we attempted to minimize the CTE mismatch between electrode and $CoSb_3$ material using the alloyed W–Cu electrodes. At the same time, one-step sintering technique of $CoSb_3$/electrode was developed by SPS and the $CoSb_3$/W–Cu element was successfully fabricated. Thermal residual stress at the $CoSb_3$/electrode interface zone was analyzed using finite element. Reliability of the $CoSb_3$/W–Cu element was evaluated through accelerated thermal aging test. Microstructure and interfacial evolution of the IMCs at the $CoSb_3$/electrode interface during thermal aging was discussed. The shear strength and electrical contact resistance of $CoSb_3$/W–Cu element were evaluated.

2. Experimental procedure

The $CoSb_3$ ingots were prepared by melting the starting materials in vacuum-encapsulated quartz tube at 1353 K followed by annealing at 863 K for 150 h. The resulting ingots were ground into powder for TE element fabrication. The $CoSb_3$/W–Cu element was sintered by SPS Apparatus (SPS-2040, Sumitomo Coal

* Corresponding author. Tel.: +86 531 84898930.
E-mail addresses: mse_zhaodg@ujn.edu.cn, degang2008@163.com (D. Zhao).

0925-8388/$ – see front matter © 2011 Elsevier B.V. All rights reserved.
doi:10.1016/j.jallcom.2011.12.130

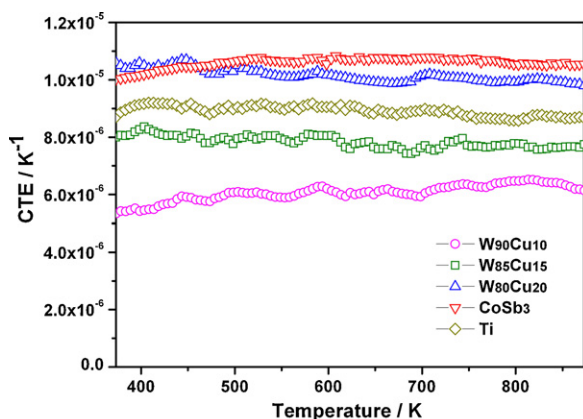

Fig. 1. Temperature dependence of the CTE for W–Cu electrodes and $CoSb_3$ TE material.

Mining Co., Tokyo, Japan). The sintering of $CoSb_3$ powder and joining of $CoSb_3$ with W–Cu electrode was simultaneously performed. The W–Cu electrodes with different contents of Cu were produced by Changsha Saneway Electronic Materials Co. Ltd., China. Titanium powder was chosen as the buffer material due to its close thermal expansion coefficient with $CoSb_3$ (shown in Fig. 1). The 1.2 mm-thickness electrode was firstly ultrasonically cleaned in ethanol and then put in the graphite die. The Ti powder was dusted on the electrode uniformly and compacted by the graphite punch. The $CoSb_3$ powder was placed on the Ti layer and then sintered by SPS method in vacuum at 863 K under pressure of 50 MPa for 600 s.

Each element of $CoSb_3$/W–Cu was cleaned with alcohol, encapsulated in vacuum quartz tube and placed in a furnace for thermal duration test. As the hot sides of $CoSb_3$-based TE device generally work at about 773 K, accelerated aging temperature, 823 K, was used in this study. The aging period ranged from 0 to 30 days. Upon completion of the aging step, the samples were then mounted in epoxy and polished in preparation for characterization. Microstructure of the $CoSb_3$/W–Cu element was observed using scanning electron microscopy (SEM, CARL ZEISS EVOMA10). The thermal residual stress of $CoSb_3$/W–Cu element was analyzed with commercial finite element ANSYS 10. The compositions of the IMC phases forming at the $CoSb_3$/Ti interface were determined by an electron probe micro-analysis (EPMA, JEOL, JXA-8100). The electrical contact resistance was measured by a four probe technique. The joints were cut into a long bar 3 mm × 3 mm × 8 mm in size and then polished in preparation for measuring the contact resistance. Shear test was performed in a tensile tester (INSTRON 5566R) at room temperature to examine the bonding strength. The load speed was 0.2 mm/min in the shear test. Shear strength of the joint was taken from the average value of five specimens.

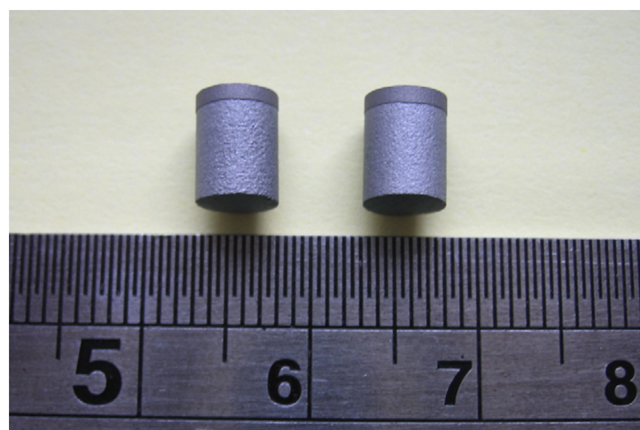

Fig. 3. Photograph of sintered $CoSb_3$/Ti/$W_{80}Cu_{20}$ TE elements.

3. Results and discussion

3.1. Fabrication of $CoSb_3$/W–Cu element

The thermal match of CTE between metal electrode and TE material is the first consideration for the construction of TE element. Fig. 1 shows the CTE of W–Cu electrodes and $CoSb_3$ material as a function of temperature. To make a comparison, the CTE of Ti is also present in Fig. 1. It can be seen that the CTE value of $CoSb_3$ ranges from 1.0×10^{-5} K^{-1} to 1.1×10^{-5} K^{-1} when temperature increases from 373 K to 873 K. Among the three kinds of W–Cu electrodes designed, the CTE of $W_{90}Cu_{10}$ electrode has the largest gap with, and is lower by about 43.4% than, that of $CoSb_3$; on the contrary, the

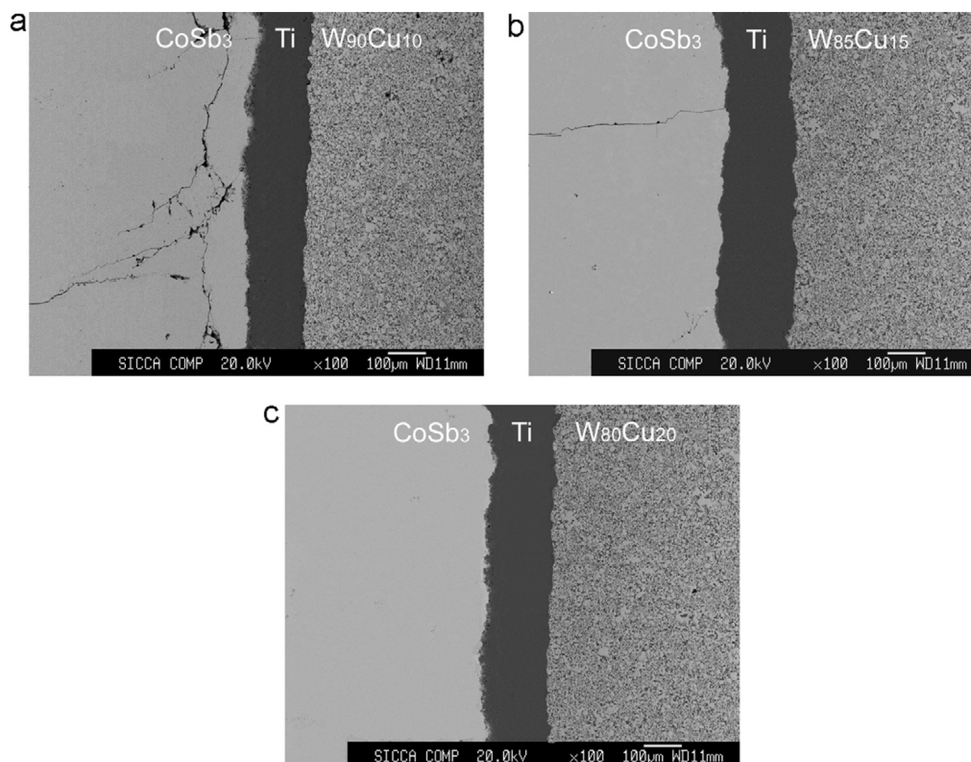

Fig. 2. SEM micrographs of the junction of $CoSb_3$/Ti/electrode joints; (a) $CoSb_3$/Ti/$W_{90}Cu_{10}$, (b) $CoSb_3$/Ti/$W_{85}Cu_{15}$ and (c) $CoSb_3$/Ti/$W_{80}Cu_{20}$.

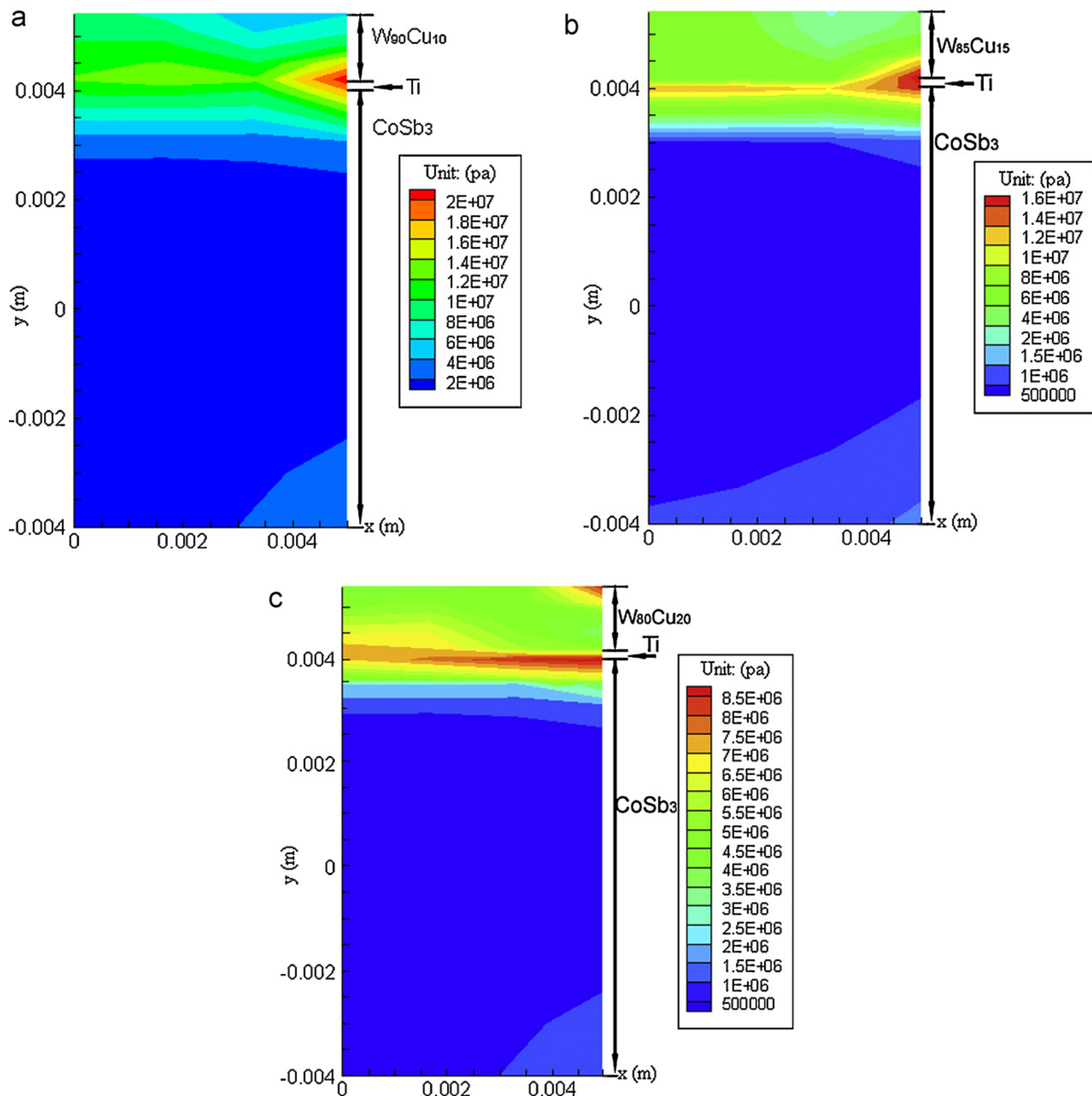

Fig. 4. The calculated thermal residual stress in $CoSb_3$/Ti/W–Cu systems; (a) $CoSb_3/Ti/W_{90}Cu_{10}$, (b) $CoSb_3/Ti/W_{85}Cu_{15}$ and (c) $CoSb_3/Ti/W_{80}Cu_{20}$.

CTE of $W_{80}Cu_{20}$ electrode has the least gap with that of $CoSb_3$ and ranges from $0.95 \times 10^{-5}\,K^{-1}$ to $1.05 \times 10^{-5}\,K^{-1}$, which is very close to that of $CoSb_3$ between 373 K and 873 K. The CTE of $W_{85}Cu_{15}$ is intermediate between those of $W_{90}Cu_{10}$ and $W_{80}Cu_{20}$. The CTE gap between $CoSb_3$ and $W_{85}Cu_{15}$ is about 26.3%. In view of reducing the thermal residual stress, the $W_{80}Cu_{20}$ is likely to be the most suitable electrode for $CoSb_3$ material. Three kinds of electrodes were used to join with $CoSb_3$ TE material using one-step SPS sintering. For a comparison, the joining process was carried out at the same condition in this study.

Fig. 2 shows the SEM micrographs of the junction of $CoSb_3$/W–Cu prepared using one-step SPS sintering. Visible cracks in $CoSb_3$ material can be seen in the joint of $CoSb_3/Ti/W_{90}Cu_{10}$, as shown in Fig. 2(a). The reason for this is related to the thermal stress resulting from the CTE difference. The CTE of $W_{90}Cu_{10}$ is lower than that of $CoSb_3$ and the tensile stress was generated during cooling inside the $CoSb_3$ adjacent to $CoSb_3$/Ti interface. When the $CoSb_3$ cannot stand the tensile stress inside the $CoSb_3$, cracks appears near the $CoSb_3$/Ti interface. Similar phenomenon was also observed at the $CoSb_3/Ti/W_{85}Cu_{15}$ interface, as shown in Fig. 2(b). However, no crack was inspected at the $CoSb_3/Ti/W_{80}Cu_{20}$ interface and the $CoSb_3$/electrode interface is well bonded, just as Fig. 2(c) shown. The results above indicated that the $W_{80}Cu_{20}$ alloy had an excellent thermal match with the $CoSb_3$ material, which was consistent with the CTE results in Fig. 1. In addition, the $W_{80}Cu_{20}$ has higher electrical and thermal conductivity than $W_{85}Cu_{15}$ and $W_{90}Cu_{10}$ due to high content of Cu. Therefore $W_{80}Cu_{20}$ electrode could be regard as a novel and suitable electrode for $CoSb_3$-based TE device. Fig. 3 shows the photograph of sintered $CoSb_3$-based TE elements.

The thermal residual stress in three kinds of $CoSb_3$/Ti/W–Cu system was calculated with an elastic ax-symmetric finite element model using ANSYS 10.0 software. The material property parameters dependent on temperature in the simulation were measured. The electrical resistivity of $CoSb_3$, Ti, W–Cu and graphite was measured by standard DC four-probe method in a flowing Ar atmosphere. The thermal conductivity of $CoSb_3$, Ti, W–Cu and

graphite was measured by laser flash method (Netzsch, LFA427). The density of material at several temperatures was calculated using the thermal expansion coefficient measured by Neztsch DIL 402C. The specific heat of $CoSb_3$ and graphite was measured by ASTM E1269-05 (PE DSC-2C), and the specific heat of W–Cu and Ti only slightly depends on temperature, therefore a constant value was used during simulation. The size of calculated model is $\varnothing 10 \times 9.3$ mm and the thickness of $CoSb_3$, Ti and W–Cu is 8, 0.1 and 1.2 mm, respectively. Fig. 4 shows the calculated thermal residual stress in three kinds of $CoSb_3$/Ti/W–Cu systems. It can be seen that the maximum thermal residual stress usually appeared at the cylindrical surface zone close to the region of $CoSb_3$/electrode interface. The maximum thermal residual stress of $CoSb_3/Ti/W_{90}Cu_{10}$, $CoSb_3/Ti/W_{85}Cu_{15}$ and $CoSb_3/Ti/W_{80}Cu_{20}$ system was about 20, 16 and 8.5 MPa, respectively. The calculated results agreed well with the experimental results.

3.2. Interfacial microstructure and evolution behavior

Thermal duration test was carried out at the serving temperature of 773 K. Fig. 5 shows the SEM micrographs at the region of $CoSb_3/Ti/W_{80}Cu_{20}$ interface after aging at 773 K for 30 days. It can be observed that an IMC layer formed at the $CoSb_3$/Ti interface. The EPMA line profiles confirmed the existence of Ti–Sb phase at the $CoSb_3$/Ti interface, just as shown in Fig. 5(a). With the help of EDS, the IMC phase was analyzed to be composed of 52.62 at.%Ti and 47.38 at.%Sb, corresponding to TiSb phase, as shown in Fig. 5(b). The TiSb binary compound may be formed by inter-diffusion reaction between Sb and Ti atoms. During the thermal duration period, Sb atom diffused into the $CoSb_3$/Ti interface under the driving force and reacted directly with Ti at the $CoSb_3$/Ti interface:

$$\mathrm{Sb + Ti \rightarrow TiSb.} \tag{1}$$

This reaction resulted in the formation of TiSb IMC layer.

When the thermal duration test was carried out at the accelerated temperature of 823 K, TiSb phase was also found after aging for 2 days. Fig. 6 shows the SEM micrographs at the region of $CoSb_3$/Ti interface of $CoSb_3/Ti/W_{80}Cu_{20}$ element aged at 823 K for various aging time. It can be observed that with the thermal duration time prolonging, the thickness of IMC layer increased. In addition, a three-layer IMC structure at the $CoSb_3$/Ti interface was observed after aging at 823 K for 30 days and the total thickness was about 20 μm. According to the results of EDS, the phase adjacent to TiSb layer was composed of 34.3 at.%Ti and 65.7 at.%Sb, corresponding to $TiSb_2$ IMC phase. The composition of IMC phase neighbored with $TiSb_2$ layer was 33.4 at.%Ti, 30.8 at.%Co and 35.8 at.%Sb, indicating a TiCoSb phase. The formation of IMC layers is mainly due to the mutual diffusion of Sb and Ti atoms under the driving force from the chemical potential. Fig. 7 shows the sketch of evolution behavior of IMCs at the $CoSb_3$/Ti/W–Cu interface during the accelerated aging. During the thermal aging period, Sb decomposed from $CoSb_3$ continued diffusing and to react with TiSb phase as:

$$\mathrm{Sb + TiSb \rightarrow TiSb_2.} \tag{2}$$

This reaction resulted in the formation of $TiSb_2$ IMC layer. Meantime, as the aging continued, Ti atoms also diffused into $CoSb_{3-x}/TiSb_2$ interface, and then the reaction occurred as:

$$\mathrm{Ti + CoSb_{3-x} \rightarrow TiCoSb.} \tag{3}$$

Therefore, the mutual diffusion of Sb and Ti resulted in the three-layer IMC structure at the $CoSb_3$/Ti interface after the accelerated aging of 30 days at 823 K.

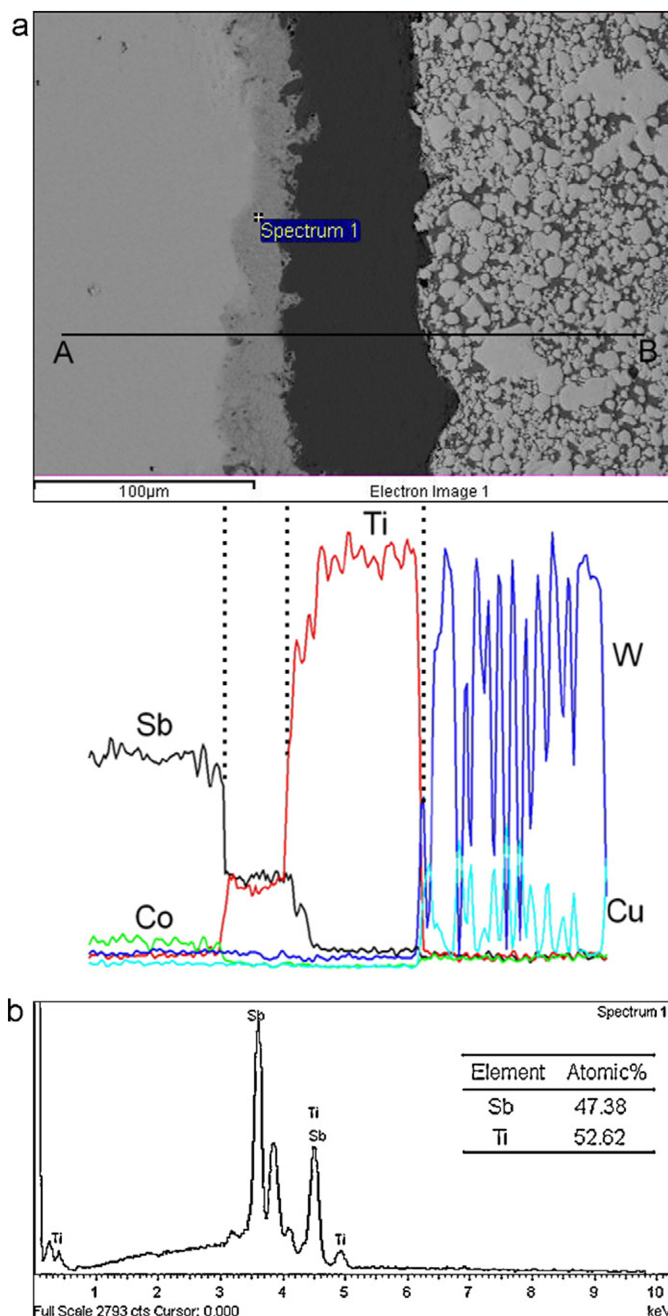

Fig. 5. (a) SEM micrograph and EPMA line analysis at the region of $CoSb_3/Ti/W_{80}Cu_{20}$ interface after aging at 773 K for 30 days and (b) EDS analysis of TiSb phase.

3.3. Mechanical properties of TE element

Many studies have been published concerning the mechanical reliability of solder joints [12–14]. It was known that excessively thick reaction layers, formed between solder and substrate, could significantly degrade the mechanical reliability of joints. In this study, IMCs formed at the $CoSb_3$/Ti interface are brittle phases and excessively thick IMC layers also made the cracks form at the $CoSb_3$/IMCs. Shear test was performed to evaluate the effect of the interfacial reactions on the reliability of the $CoSb_3$/electrode joints as a function of accelerated aging time. Fig. 8 shows the variation of the shear strength with the aging time. The shear strength significantly decreased after accelerated aging for initial 192 h and

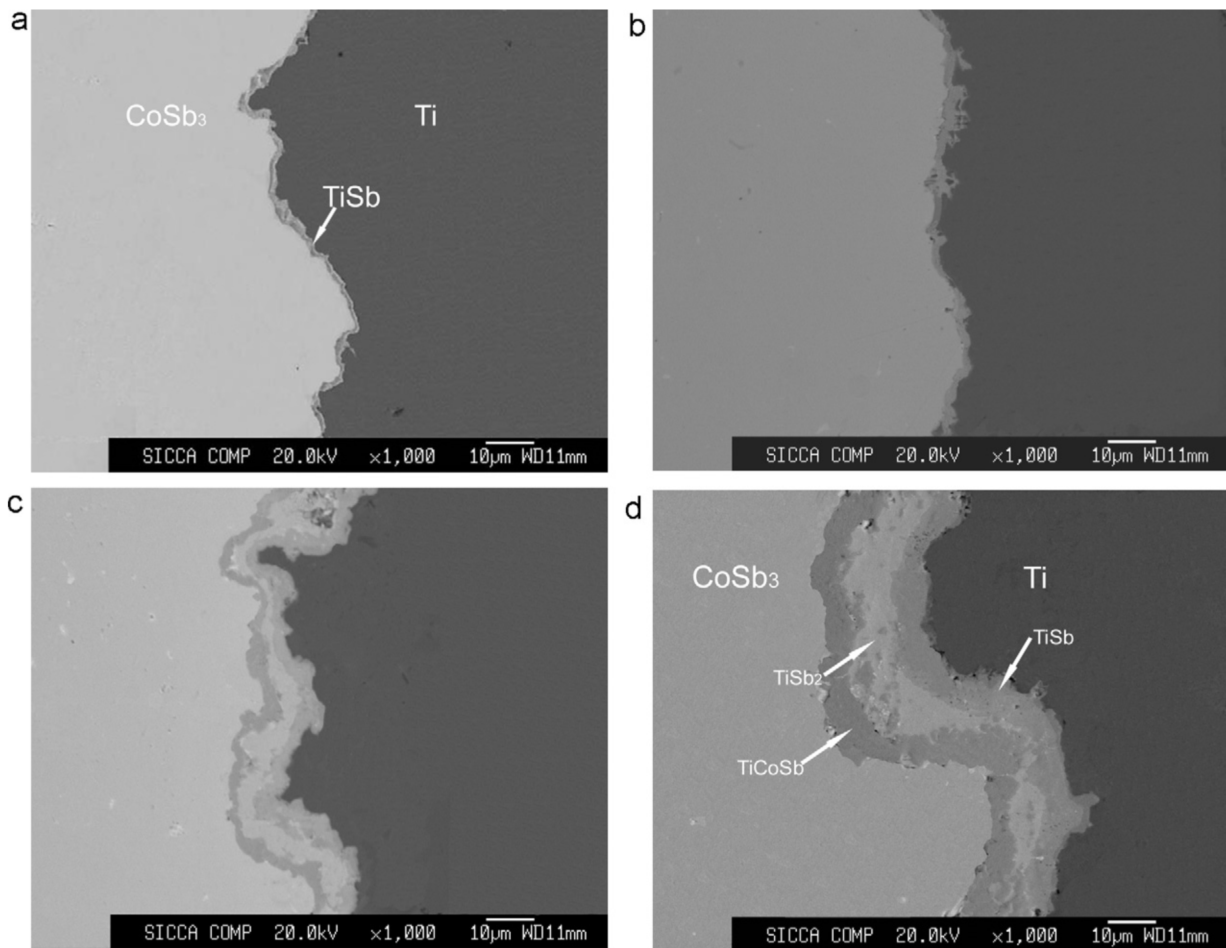

Fig. 6. SEM micrographs at the $CoSb_3$/Ti interface of $CoSb_3$/Ti/W–Cu joints after thermal aging at 823 K for various aging time; (a) 2 days, (b) 8 days, (c) 20 days and (d) 30 days.

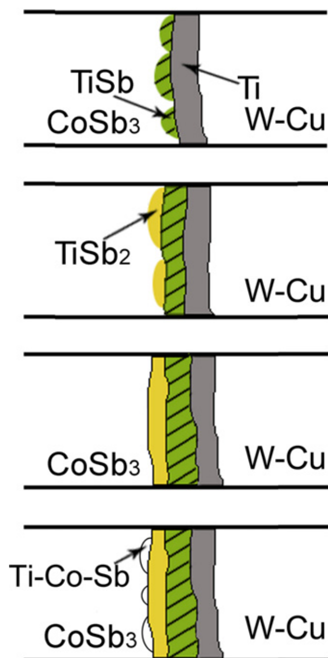

Fig. 7. Schematic illustration of the interfacial evolution at the $CoSb_3$/Ti/W–Cu interface during thermal aging.

then slightly decreased with the aging time increasing. The average shear strength of the joints before accelerated aging was about 52 MPa. Compared to the strength measured before aging, the shear strengths decreased by 47.3% after accelerated aging at 823 K for 192 h. The average shear strength of the joints after accelerated aging at 823 K for 720 h was about 17 MPa which is sufficient for mechanical reliability of TE device.

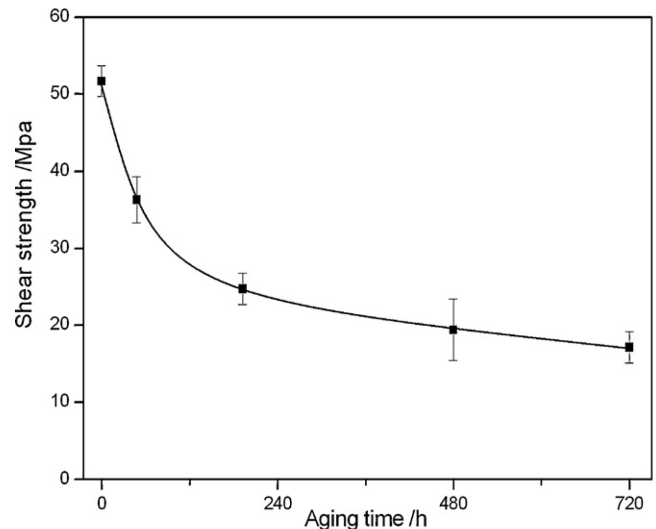

Fig. 8. Shear strength of $CoSb_3$/Ti/W–Cu joints with the aging time.

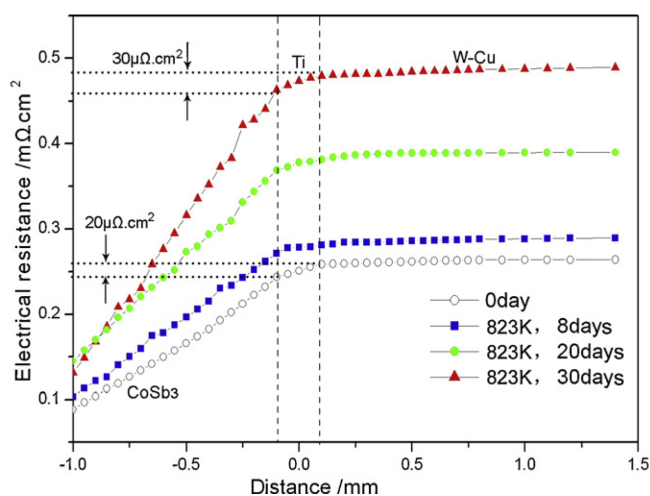

Fig. 9. Electrical contact resistance of the $CoSb_3/Ti/W_{80}Cu_{20}$ thermoelectric element.

3.4. Electrical contact properties of TE element

Good electrical contact between $CoSb_3$ and electrode is important for the efficiency of TE device. Fig. 9 shows the electrical contact resistance of the $CoSb_3/Ti/W_{80}Cu_{20}$ thermoelectric element. The results show that the interfacial contact resistance of $CoSb_3/Ti/W_{80}Cu_{20}$ was about 20 $\mu\Omega\,cm^2$. After thermal aging at 823 K for 30 days, the contact resistance was still minimal and about 30 $\mu\Omega\,cm^2$. It is concluded that the growth of IMC layers formed between $CoSb_3$ and W–Cu electrode may result in the increase of contact resistance. The value of the contact resistance was almost same with that of commercial bismuth telluride device with Sn–Pb solder [15]. These results showed that the electrical contact of $CoSb_3/Ti/W_{80}Cu_{20}$ TE element was good. The $CoSb_3/Ti/W_{80}Cu_{20}$ TE elements have excellent thermal duration stability.

4. Conclusions

A suitable W–Cu alloy electrode was introduced into $CoSb_3$-based element with insertion of Ti layer by means of spark plasma sintering. The $CoSb_3/TiW_{80}Cu_{20}$ TE element was successfully fabricated. The maximum thermal residual stress appeared at the cylindrical surface zone close to the $CoSb_3$/electrode interface. An IMC layer formed at the $CoSb_3$/Ti interface. After accelerated thermal aging, a three-layer IMC structure composed of TiCoSb, $TiSb_2$ and TiSb formed at the $CoSb_3$/Ti interface. The $CoSb_3/Ti/W_{80}Cu_{20}$ elements have sufficient shear strength and good electrical contact for the reliability of thermoelectric device.

Acknowledgements

This work was supported by Natural Science Foundation of Shandong Province of China Granted No. ZR2011EMQ006, Jinan Science and Technology Stars Funds Granted No. 20100310 and Doctoral Fund of University of Jinan Granted No. XBS12.

References

[1] R. Funahashi, M. Mikami, T. Mihare, S. Urata, N. Ando, J. Appl. Phys. 99 (2006) 066117.
[2] Y.P. Jiang, X.P. Jia, T.C. Su, N. Dong, H.A. Ma, J. Alloys Compd. 493 (2011) 535.
[3] M. Orihashi, Y. Noda, L.D. Chen, Y.S. Kang, A. Moro, T. Hirai, Proc. 17th Inter. Conf. on Thermoelectrics, IEEE, Nagoya, Japan, 1998, p. 543.
[4] K. Hasezaki, H. Tsukuda, A. Yamada, S. Nakajima, Y. Kang, M. Niino, Proc. 16th Inter. Conf. on Thermoelectrics, IEEE, Dresden, Germany, 1997, p. 599.
[5] J.J. Zhang, B. Xu, F.R. Yu, D.L. Yu, Z.Y. Liu, J. Alloys Compd. 503 (2010) 490.
[6] L. Zhang, N.M. Koblyuk, E. Royanian, A. Grytsiv, P. Rogl, J. Alloys Compd. 504 (2011) 53.
[7] Z. Xiong, X.H. Chen, X.Y. Huang, S.Q. Bai, L.D. Chen, Acta Mater. 58 (2010) 3995.
[8] P.F. Qiu, X. Shi, X.H. Chen, X.Y. Huang, L.D. Chen, J. Alloys Compd. 509 (2011) 1101.
[9] M.S. Elgenk, H.H. Saber, T. Caillat, J. Sakamoto, Energy Convers. Manage. 47 (2006) 174.
[10] H.S. Chun, J.W.S. Yoon,.B. Jung, J. Alloys Compd. 439 (2007) 91.
[11] D.G. Zhao, X.Y. Li, W. Jiang, L.D. Chen, J. Alloys Compd. 477 (2009) 425.
[12] Y.H. Lee, H.T. Lee, Mater. Sci. Eng. A 444 (2007) 75.
[13] J.W. Yoon, S.B. Jung, J. Alloys Compd. 458 (2008) 200.
[14] Y.T. Chin, P.K. Lam, H.K. Yow, T.Y. Tou, Microelectron. Reliab. 48 (2008) 1079.
[15] C.N. Liao, C.H. Lee, W.J. Chen, Electrochem. Solid-State Lett. 10 (2007) 23.